17th World Conference on Earthquake Engineering, 17WCEE
Sendai, Japan - September 27th to October 2nd, 2021

ON THE BAYESIAN ETAS FORECASTING AND SHORT-TERM PSHA OF THE JUNE 2000 AFTERSHOCK SEQUENCE IN SOUTH ICELAND

A. Darzi [(1)], B. Halldórsson [(2,3)], B. Hrafnkelsson [(4)], H. Ebrahimian [(5)], F. Jalayer [(6)]

[(1)] *Postdoctoral Research Associate, Faculty of Civil and Environmental Engineering, University of Iceland, atefe@hi.is*
[(2)] *Research Professor, Faculty of Civil and Environmental Engineering, University of Iceland, skykkur@hi.is*
[(3)] *Earthquake and Engineering Seismology Specialist, Division of Processing and Research, Icelandic Meteorological Office*
[(4)] *Professor, Faculty of Physical Sciences, University of Iceland, birgirhr@hi.is*
[(5)] *Assistant Professor, Department of Structures for Engineering and Architecture, University of Naples Federico II, ebrahimian.hossein@unina.it*
[(6)] *Associate Professor, Department of Structures for Engineering and Architecture, University of Naples Federico II, fatemeh.jalayer@unina.it*

Abstract

Iceland is the most seismically active region in northern Europe. The largest earthquakes in Iceland occur within the two transform fault zones in the country, the more populous of which is the South Iceland Seismic Zone (SISZ). Intense aftershock sequences followed the two largest and recent earthquakes in SISZ and Reykjanes Peninsula Oblique Rift (RPOR), M_w6.4 17 June and M_w6.5 21 June 2000 earthquakes. In the aftermath of a strong earthquake, aftershocks tend to cluster in time and space, forming complex earthquake sequences that complicate the assessment of the temporal variation of probabilistic seismic hazard of aftershock greatly. In fact, modelling spatio-temporal aftershock clustering is one of the first steps towards a more detailed and improved short-term (i.e., days, weeks) risk forecasting, loss prevention, emergency disaster management and response. The statistical seismicity-based forecasting models such as the epidemic-type aftershock sequence (ETAS) [1] provide an opportunity to evaluate the feasibility of short-term seismicity forecasts and the resulting short-term probabilistic seismic hazard predictions.

This study is carried out to evaluate the feasibility of operational earthquake forecasting of aftershocks for localities in the SISZ by anticipating the characteristics of the aftershock sequences that follow damaging earthquakes in the SISZ and determining the corresponding evolving seismic hazard in the short-term. To this end, we retrospectively provide forecasts of the spatial distribution of events within a prescribed forecasting time window (24-hour and 1-week intervals) during the June 2000 aftershock sequence using a fully simulation-based procedure [2]. The method is based on a well-established Bayesian spatio-temporal ETAS model which enables estimation of the model parameters while accounting for their uncertainties in a robust manner through posterior joint probability distributions. The forecasted short-term seismicity rates from the Bayesian ETAS model are directly incorporated into the seismic hazard framework [3]. We obtain the short-term rate of exceeding peak ground acceleration (PGA) threshold at the locality of Hveragerði-town in the SISZ and compare the results with the seismic hazard values obtained from long-term seismicity values incorporated in the classic probabilistic seismic hazard assessment (PSHA, e.g. [4]). To this end, the probability gain values are provided for the studied scenarios. To capture the epistemic uncertainty in aftershock hazard assessment, local ground motion prediction equations (GMPEs) (i.e. [5, 6]) and different maximum magnitude values are employed. The comparison shows that the short-term hazard values increase by 10 to 500 depending on the PGA, forecasting interval duration, and corresponding starting time during the aftershock sequence in the SISZ. The probability gain factor is most significant for shorter (one-day) forecasting intervals after the 17 June large earthquake.

Keywords: short-term PSHA; aftershock sequence; ETAS; Bayesian; operational earthquake forecasting

1. Introduction

In Iceland, the most significant earthquakes take place in the two major transform zones of the country, one of which is the South Iceland Seismic Zone (SISZ), where earthquakes up to M_w7.0 have occurred and caused damage in the predominantly flat rural agricultural region with a few small towns but all critical infrastructure and lifelines of modern-day society. Intense aftershock sequences followed the two largest and recent earthquakes in SISZ, namely M_w6.4 of 17 June 2000 and M_w6.5 of 21 June 2000 earthquakes.

To improve preparedness measures within an ongoing seismic sequence and consequently predict expected losses in the affected area, providing detailed hazard forecasting is the first essential action; it helps the first responders and decision-makers such as civil protection agencies informed decisions [7]. For this reason, the establishment of an operational earthquake forecasting (OEF) system is necessary to deliver timely seismicity (in terms of spatio-temporal occurrence of seismic events) and hazard (in terms of rate of exceeding prescribed levels of seismic ground-shaking) forecasting information [8].

The Epidemic-Type Aftershock Sequence (ETAS) model clusters aftershocks in space and time [1]. The ETAS family models are proved to be one of the best models in describing the spatio-temporal distribution of observed seismicity, especially in short-term time window [8–10]. Furthermore, they are widely used in OEF systems and incorporated within the probabilistic seismic hazard assessment studies (PSHA) [8, 11–13]. Admittedly, one of the main challenges of using the ETAS model is estimating the model parameters, which is affected by a large amount of uncertainty [2, 14, 15]. One of the key advantages of the Bayesian parameter estimation method that makes it preferable over the conventional time-independent methods [3, 16] is the capability of quantifying the uncertainties associated with the model parameters. In the Bayesian approach, the posterior distribution of every model parameter can be acquired; thereby, more and richer information about parameters can be extracted, while in the conventional methods only single-point estimates are determined. Omi *et al.* [16,17] employed a Bayesian approach to use many sets of possible parameter distribution for a forecasting model and found the procedure sufficient for aftershock forecasting for a potential OEF system in Japan. Ebrahimian and Jalayer [2] proposed a fully simulation-based approach to provide a robust spatio-temporal seismicity forecast employing a Bayesian parameter estimation procedure to account for the epistemic uncertainty of ETAS model parameters. The method was retrospectively tested on the 2016 Amatrice-Norcia seismic sequence in central Italy [2] and also provided promising results for the South Iceland earthquakes in 2000 [17].

Recently, Hardebeck *et al.* [18] updated the aftershock forecasting model parameters of [19] for the recent seismic earthquakes in California for contribution to the operational aftershock forecasting presented in U.S. Geological Survey [20]. For this purpose, they have exploited the Bayesian updating procedure. Most recently, Shcherbakov *et al.* [21] proposed a methodology based on the Bayesian approach and the extreme value theory to forecast the magnitude of the likely intense earthquake. They retrospectively tested their proposed model's applicability in the 2016 Kumamoto, Japan, earthquake sequence using ETAS to model earthquake occurrence.

Seismic aftershock hazard forecasts, provided in terms of the mean short-term (e.g. hourly/daily/weekly) rate of exceeding prescribed levels of ground-shaking, rely on the spatio-temporal aftershock triggering model, and a ground motion prediction equation (GMPE). A reliable selection of a set of appropriate GMPEs for each region needs a comprehensive study through data-driven ranking procedures. The previous PSHA studies in Iceland are limited, as some ignore the effect of epistemic uncertainty as they are only based on a single GMPE, or use a GMPE having too simplistic functional form, or use a logic-tree approach with several GMPEs that turn out to be inappropriate ones that do not capture the characteristics of Icelandic strong-motion [see in 22, 23]. To address these shortcomings, a set of new empirical Bayesian GMPEs have been proposed for Icelandic strong-motions that fully capture their characteristics [5].

In this work, the spatial aftershock forecasts are generated for one-week and one-day forecasting intervals following the two large earthquakes of 17 and 21 June 2000 starting 4 hours after their occurrence, along with the uncertainty associated with the generated forecasts. To this end, a Bayesian spatio-temporal

ETAS model [2] is employed. Following that, the short-term PSHA is performed to assess the increase in the short-term rate of exceeding various PGA thresholds at the location of the town of Hveragerði in the SISZ, that happened to be in the extreme near-fault region of the M_w6.3 of 29 May 2008 Ölfus earthquake [24, 25]. To compare the short-term results with the long-term hazard values obtained from the conventional PSHA, their ratio (i.e., probability gain) is displayed as function of PGA thresholds.

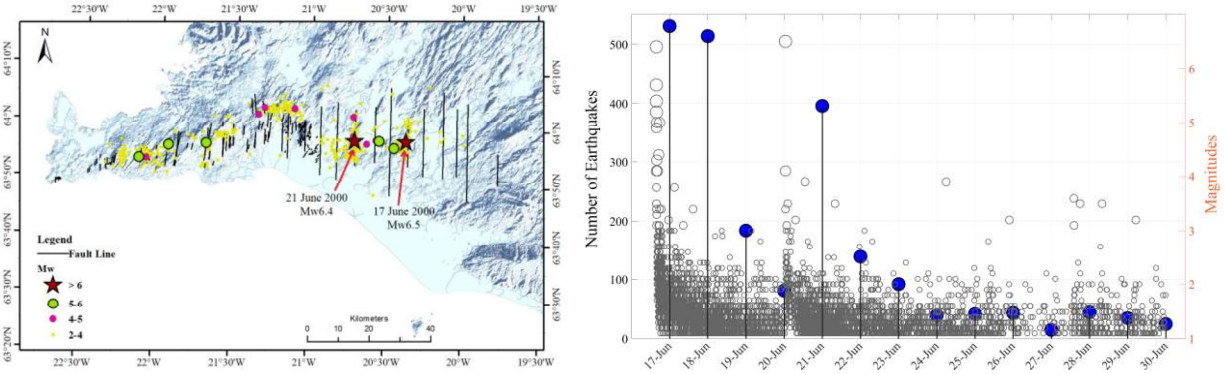

Fig. 1 – Left panel: geographical distribution of the June 2000 seismic sequence across Southwest Iceland from 17-30 June 2000, with different symbols denoting the magnitude ranges. The 17 and 21 June 2000 earthquake epicentres are depicted by red stars. The revised catalogue used is from Panzera *et al.* [26]. The black lines show the faults in the SISZ and RPOR, according to [27–29]. Right panel: temporal distribution of the 2000 sequence. The circles' diameter is proportional to the corresponding earthquake magnitude (right y-axis). The daily number of events with $M_w \geq 1.5$ are indicated by blue circles (left y-axis).

2. Method

2.1 Short-term seismicity forecasting methodology

Short-term seismicity forecasts are computed using a spatio-temporal ETAS model whose parameters are updated within an ongoing seismic sequence [2]. Using Eq. (1), we obtain the average number of events in the spatial cell centred at a location of (x, y) with magnitude larger than or equal to m that is expected to take place in the time interval of $[T_{start}, T_{end}]$, denoted as $N(x, y, m \mid \mathbf{seq}, M_{cut})$. The expected number of events E[N] is calculated given 1) observation history of earthquakes that occurred prior to the T_{start}, denoted as **seq**, and 2) the lower cut-off magnitude, M_{cut}.. N_b represents the background seismicity which is often considered to be time-independent. λ is the spatio-temporal ETAS clustering model employing a series of events that taken place prior to the prescribed forecasting interval and the sequence of events expected to happen during the forecasting interval (denoted as $\mathbf{seq}_g$ hereafter). The term $p(\mathbf{seq}_g \mid \boldsymbol{\theta}, \mathbf{seq}, M_{cut})$ is the probability distribution function (PDF) for $\mathbf{seq}_g$, the sequence of events that is expected to occur during the forecasting time interval of $[T_{start}, T_{end}]$, given $\boldsymbol{\theta}$, **seq** and M_{cut}. The term $p(\boldsymbol{\theta} \mid \mathbf{seq}, M_{cut})$ is the conditional PDF for $\boldsymbol{\theta}$ given the known **seq** and M_{cut}. $\boldsymbol{\theta}$ is the vector of ETAS model parameters.

$$N(x,y,m|\,\mathbf{seq},M_{\mathrm{cut}}) = N_{\mathrm{b}}(x,y,m|M_{\mathrm{cut}}) + \int_{\Omega_{\boldsymbol{\theta}}}\left[\int_{\Omega_{\mathbf{seq}_{\mathrm{g}}}}\int_{T_{\mathrm{end}}}^{T_{\mathrm{start}}}\left(\lambda\left(t,x,y,m\middle|\mathbf{seq}_{\mathrm{g}},\boldsymbol{\theta},\mathbf{seq},M_{\mathrm{cut}}\right)\mathrm{d}t\right).p\left(\mathbf{seq}_{\mathrm{g}}\middle|\boldsymbol{\theta},\mathbf{seq},M_{\mathrm{cut}}\right)\mathrm{d}\mathbf{seq}_{\mathrm{g}}\right].p(\boldsymbol{\theta}|\mathbf{seq},M_{\mathrm{cut}})\mathrm{d}\boldsymbol{\theta} \quad (1)$$

$\lambda()$ describes the rate of occurrence of earthquakes at a specific time t elapsed after the mainshock's origin time. As shown in Eq. (2), λ_{ETAS} accounts for the triggering effect of the events with $M_j \geq M_{cut}$ that happened at $t_j < t$ prior to the desired forecasting interval given **seq**, $\boldsymbol{\theta}$ and M_{cut}. $\mathbf{seq}_t$ expressed by $\mathbf{seq}_t = \{(t_j, x_j, y_j, M_j), t_j < t, M_j \geq M_{cut}\}$, includes a series of observed earthquakes with magnitude larger than or equal to M_{cut} occurred up to the time t, which are indicated by j subscript in Eq. (2). r_j is the distance between the earthquake j and the cell centre (x, y). As expressed by Eq. (2), the triggering function comprised of three empirical relationships, (1) the productivity of an earthquake to generate series of aftershocks according to the Gutenberg—Richter relationship, modelled by the parameters β, K, K_t and K_R, (2) temporal distribution

of triggered earthquakes based on the modified Omori law modelled by c and p, and (3) the spatial distribution of events characterized by d and q parameters. The vector $\boldsymbol{\theta}$ includes [β, c, p, d, q, K, K_R, and K_t], the first five parameters are the main ETAS parameters, and the rest, namely, K, K_R, and K_t are calculated as functions of the main parameters. Interested readers are encouraged to see [2] for a detail description of the spatio-temporal model.

$$\lambda_{\mathrm{ETAS}}(t,x,y,m|\boldsymbol{\theta},\mathbf{seq}_t,M_{\mathrm{cut}}) = e^{-\beta(m-M_{\mathrm{cut}})}\sum_{t_j<t} K.e^{\beta(M_j-M_{\mathrm{cut}})}.\frac{K_{\mathrm{t}}}{(t-t_j+c)^p}.\frac{K_{\mathrm{R}}}{(r_j^2+d^2)^q} \qquad (2)$$

The first step in the Bayesian seismicity forecasting framework is to assign a prior distribution to each main ETAS model parameters. In this study, a normal probability distribution is selected as prior distribution for each ETAS parameter, a set of optimal space-time ETAS model parameters proposed by Darzi *et al.* [17] is used as the mean values along with the constant coefficient of variation (CV) of 0.3. The prior mean values are set to β =1.08, c =0.005, p =1.197, and d =0.87, q =1.602. It should be noted that while these values were obtained by calibrating the Bayesian ETAS model to the June 2000 seismic sequence itself, the focus is on the effects of forecasted short-term seismicity relative to the background seismicity.

According to the Bayesian seismicity forecasting approach (as per [2, 17]), in the next step, samples of $\boldsymbol{\theta}$ are generated from the posterior PDF of $p(\boldsymbol{\theta} \mid \mathbf{seq}, M_{\mathrm{cut}})$ using the MCMC simulation routine [30, 31], and the Metropolis-Hastings algorithm [32, 33]. Note that 10% of the first iterations, known as the burn-in, is discarded from the generated samples.

After sampling $\boldsymbol{\theta}$, to generate plausible seismic sequences for the prescribed forecasting interval ($\mathbf{seq}_g$) given the sampled values of $\boldsymbol{\theta}$, **seq** and M_{cut}, a stochastic simulation-based procedure is adopted [2]. In other words, $\mathbf{seq}_g$ is generated based on the PDF $p(\mathbf{seq}_g \mid \boldsymbol{\theta}, \mathbf{seq}, M_{\mathrm{cut}})$. Finally, robust estimates of $N(\cdot)$ are obtained corresponding to various magnitude thresholds at each grid cell. Hence, the seismicity forecasting maps can be produced for a given value of m. Using the piece-wise stationary non-homogeneous Poisson process, we forecast the probability of experiencing at least one earthquake with magnitude equal to or larger than m for the entire aftershock zone by integrating the $N(x, y, m \mid \mathbf{seq}, M_{\mathrm{cut}})$ of cells in the affected area. It is worth noting that employing the Bayesian parameter estimation technique enables us to compute 2nd, 16th, 50th, 84th and 98th percentiles of $N(x, y, m \mid \mathbf{seq}, M_{\mathrm{cut}})$ at each spatial cell unit. In the next section, the median of the estimated number of events with $M > 4.5$ corresponding to the short-term (daily and weekly) intervals are employed as the seismicity rate in the PSHA framework.

2.2 Short-term seismic hazard forecasting

In this study, the seismic hazard calculation is performed at the centre of Hveragerði town with the geographical coordinate of 64.00ºN and -21.19ºW. The short-term (weekly/daily) forecasts of the aftershock hazard expressed as the short-term rate of exceeding a given PGA is obtained based on Eq. (3):

$$\lambda(PGA > z|\mathbf{seq}) = \sum \lambda(M > Mmin|\mathbf{seq}) \int_{Mmin}^{Mmax} \int_{R} P(PGA > z|m,x,y).f_M(m).f_R(x,y).dm.dx.dy \qquad (3)$$

where $\lambda(\mathrm{PGA} > z \mid \mathbf{seq})$ is the short-term rate that PGA exceeds a prescribed threshold value of z given the **seq** of the interested forecasting interval. $\lambda(M > Mmin \mid \mathbf{seq})$ is the forecasted number of events with a magnitude larger than $Mmin$ for each cell in the aftershock zone which can be expressed as $N(x, y, Mmin \mid \mathbf{seq}, M_{\mathrm{cut}})$. $f_M(m)$ is the PDF of magnitude calculated following the Gutenberg-Richter relationship. Note that the b-value is set to 0.8 for the majority of the aftershock zone cells and $Mmin$ is set to 4.5. $f_R(x,y)$ is the PDF of source-to-site distance, i.e., the distances between the Hveragerði site and all cells within the aftershock zone for which the daily/weekly seismicity forecasts are available from the previous section, are determined. $p(\mathrm{PGA} > z \mid m, x, y)$ is the probability model for ground motion prediction assessed by GMPEs.

For many hazard applications, various influential parameters are handled best by exploiting multiple values in a logic tree framework. The most considerable contributions to the overall uncertainties of seismic hazard studies are associated with the selection of appropriate GMPE. Kowsari *et al.* [22] addressed several GMPEs that have previously been used in PSHA practices in Iceland using different data-driven ranking methods and illustrated that the GMPEs developed exclusively from the Icelandic ground motion database perform best. In contrast, the others are significantly inconsistent with the actual observed earthquake data. In this study, the only two local GMPEs developed so far for Iceland, namely, Rupakhety and Sigbjörnsson [6], hereafter RS09, and Kowsari *et al.* [5], hereafter Kea20 are adopted with the weight of 50% in the logic tree framework. While strictly speaking, only the Kea20 satisfies the minimum requirements proposed by Cotton *et al.* [34] and Bommer *et al.* [35] for choosing the most robust GMPEs acceptable for PSHA, we use RS09 also as local GMPEs are very few. RS09 and Kea20 are based on Joyner-Boore distance which is the distance from the site to the surface projection of the causative fault. The soil type at the site of interest is assumed to be rock. Finally, having the short-term rate of exceedance from Eq. (3), the short-term probability of exceedance is obtained as a Poisson process.

To illustrate the level of increase in hazard value in a short time-window following a large earthquake, the exceedance rates of PGAs are calculated using a conventional PSHA framework. In the present work, a kernel-smoothed, zonation-free stochastic earthquake rate model considering SEIsmicity and accumulated FAult moment (SEIFA), developed as part of the 2013 European Seismic Hazard Model (ESHM13), is employed to extract the occurrence of earthquake activity for the conventional (long-term) PSHA computation to be compared with the short-term PSHA results. In the SEIFA-model, seismic activity rates (i.e., $\lambda(M > Mmin)$) are determined based on the frequency–magnitude distribution model of the SHARE European earthquake catalogue, while the spatial distribution of model rates depends on the density distributions of earthquakes and fault slip rates [36]. Moreover, the area source model, called AS-model, is used to obtain seismicity parameters, faulting mechanism, maximum and minimum magnitudes, hypocentral depths, and other required parameters for the PSHA practice [36]. To have a reliable comparison between the long-term and short-term PSHA results, the source parameters used in both analyses are assumed equal except the seismicity rate values which was expressed by $\lambda(M > Mmin \mid \mathbf{seq})$ (see Eq. (3)) in the short-term hazard computation.

3. Applicability to the 2000 aftershock sequence

The June 2000 seismic sequence begins with the occurrence of M_w6.4 earthquakes on 17 June at 15:40 UTC in the eastern SISZ and immediately extends towards western SISZ and Reykjanes Peninsula Oblique Rift (RPOR) [29, 37]. Three and half days later (on 21 June), 21 km to the west of the 17 June large earthquake, a M_w6.5 earthquake happened at 00:51 UTC. The left panel of Fig. 1 shows the geographical distribution of the June 2000 seismic sequence across SISZ and RPOR, following the 17 June mainshock up to 30 June 2000 characterized by different symbols corresponding to magnitude ranges. The figure indicates the increased seismicity in the whole of southwest Iceland. Red stars depict the 17 and 21 June earthquakes. Both earthquakes were caused by pre-existing right-lateral strike-slip faults with 15 km-long surface ruptures in N-S strike. This is also apparent from Fig. 1 where the micro-event clusters are accumulated in the N-S direction of the causative faults [38]. The SISZ is characterized by the bookshelf faulting model containing seismogenic strike-slip N-S striking faults. The plate movements in the region can produce earthquakes with magnitude ranging from 6.0 to 6.5 with return periods of a few decades [27, 39–42].

The Icelandic Seismic Network stations recorded the dependent shocks of the double large earthquake of June 2000 down to magnitude zero. In the present study, we used the complete earthquake catalogue provided by Panzera *et al.* [26]. The right panel of Fig. 1 indicates the temporal distribution of the 2000 seismic sequence. The circles' diameter is proportional to the corresponding earthquake magnitude (see right y-axis). The daily number of events with $M_w \geq 1.5$ are indicated by blue circles (see left y-axis). More than 500 events with $M_w \geq 1.5$ occurred on 17 and 18 June, and about 400 events with $M_w \geq 1.5$ happened on 21 June 2000. From the figure, it is explicitly clear that the seismicity decays very fast as the number of daily

aftershocks drastically decreases to less than 100 events after a couple of days. In this study, M_{cut} is calculated based on two procedures introduced to determine the magnitude of completeness of a given **seq** catalogue. The methods are based on the conventional linear regression analysis and the Bayesian estimation of the *b*-value introduced by Ebrahimian *et al.* [13]. Note that the desired M_{cut} of **seq** for the forecasting intervals is set to 2.0 for the forecasting analyses of this study. Herein, we present the results of M_{cut} calculation for the weekly interval starting ~4 hours after the occurrence of the 17 June large event.

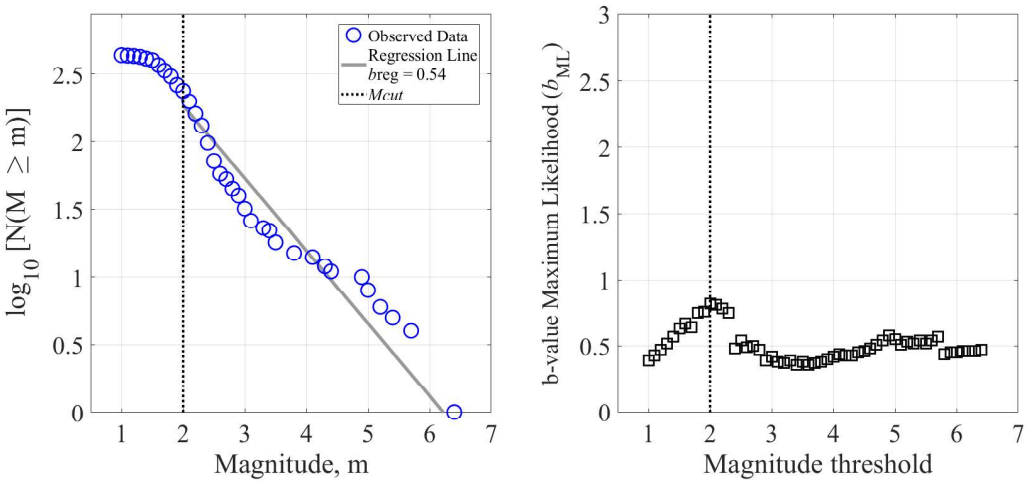

Fig. 2 – Magnitude of completeness M_{cut} calculation for the weekly forecasting interval starting ~4 hours after the occurrence of the 17 June large earthquake using two methods: conventional linear fitting (left panel) and Bayesian updating approach proposed by [13] (right panel).

4. Results

In the present work, we explore the capability of the Bayesian space-time ETAS model in short-term forecasting of the June 2000 aftershock sequence by retrospective testing of the increased seismicity in the affected area. To this end, we first provide the seismicity forecast map for entire southwest Iceland following the 17 and 21 June 2000 mainshocks and subsequently determine the increased seismic hazard values at the Hveragerði site. We generate the seismicity forecasts for SW-Iceland for two forecasting intervals of 24-hours (daily) and seven-days (weekly) starting ~ 4 hours elapsed after the occurrence of the 17 June and 21 June mainshocks.

4.1 Forecasted seismicity maps

Fig. 3 and Fig. 4 show the spatial distribution of weekly and daily seismicity forecasts for earthquakes with $M_w \geq 2.0$ starting ~ 4 hours after the occurrence of the first and second large earthquakes, respectively. The 50th percentile of the forecasted seismicity for earthquakes larger than or equal to 2.0 is exhibited (see the colour bar). The darker colour (black) shows the elevated seismicity in the aftershock area. Consistent with previous studies, the series of strong earthquakes on 17 June, i.e. the mainshock and its immediate moderate-to-large aftershocks, drastically increased the seismicity in the whole SISZ and RPOR.

As indicated in the legend, the actual observed events with $M_w \geq 2$ that happened during the corresponding forecasting intervals are depicted with markers corresponding to different M_w ranges. There is good agreement between the estimated area with increased seismicity and geographical distribution of the actual events taking place during the desired forecasting interval. $pr(M \geq m)$, m=2.0, 4.5, 5.5, and 6.5 presents the estimated probabilities of experiencing at least one earthquake exceeding the m magnitude thresholds across the whole aftershock zone. The error bar placed in the right bottom corner of the seismicity forecasts map shows the median (grey-colour square), the 16th and 84th percentiles (blue numbers) and the 2nd and 98th percentiles (black numbers) of the forecasted number of earthquakes with $M_w \geq 2$ corresponding to

the forecasting interval as reported at the top of each forecasts map. The red number (red star in error bar) notes the number of actual events during the corresponding forecasting interval.

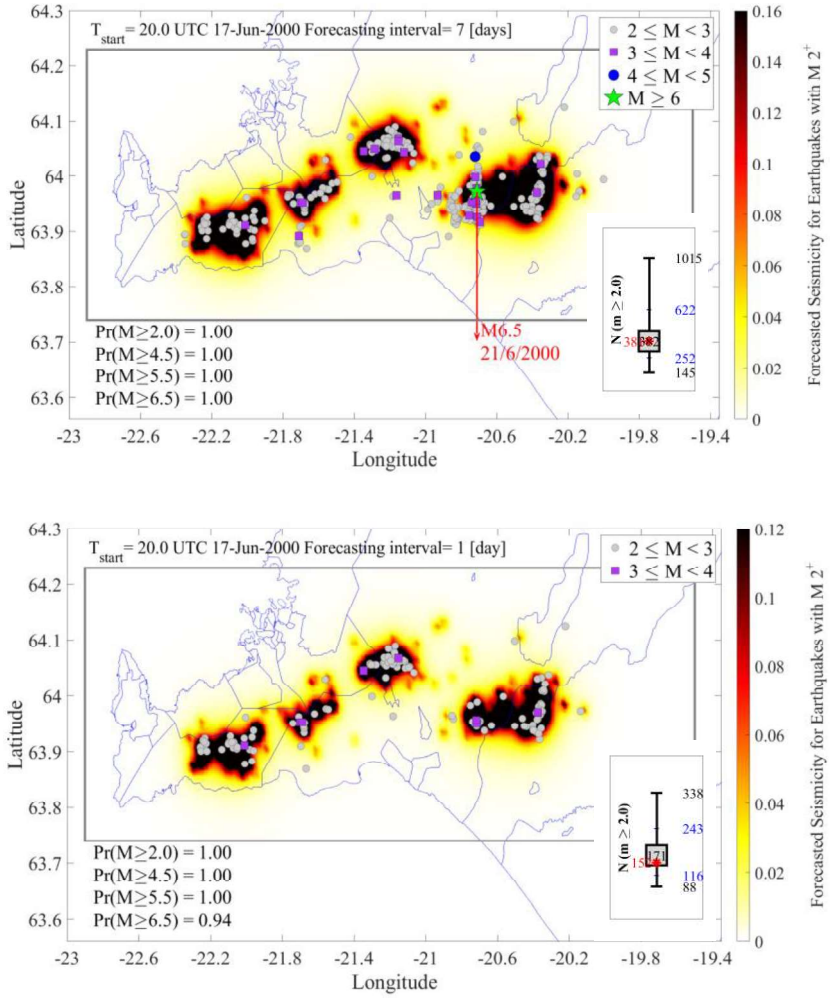

Fig. 3 – Weekly (top map) and daily (bottom map) seismicity forecasts for earthquakes with $M_w \geq 2.0$ across SISZ and RPOR following the 17 June 2000 large earthquake. The forecasting intervals start ~4 hours after the occurrence of the mainshock. As indicated in the legend, markers indicate the actual earthquakes in the aftershock zone during the prescribed forecasting interval (see the map's title). $pr(M \geq m)$, m=2.0, 4.5, 5.5, and 6.5 presents the forecasted probabilities of at least one earthquake exceeding the m magnitude thresholds in the whole SW-Iceland region.

The results prove the satisfactory performance of the advanced Bayesian ETAS model, especially after the first large earthquake, where large number of aftershocks immediately followed the mainshock (see Fig. 3). Moreover, daily aftershock forecasts of the second large shock are in remarkable agreement with the observed number of events with $M_w \geq 2$ as the actual number of events is in the 16th percentile of the predicted number of events. According to Fig. 4, regarding the weekly forecasting, the spatio-temporal ETAS seismicity model shows acceptable performance in predicting the number of events after the second large mainshock while its performance is remarkable in daily forecasting. This is chiefly because of the very fast decay of ground motions in south Iceland. Hence, the authors believe that shorter forecasting time intervals are preferable for short-term forecasting in the SW-Iceland region. It should be noticed that the median of the estimated number of events for a one-week forecasting interval starting at 20:00 UTC on 17 June (equal to 382) is almost similar to the observed number of events across the aftershock zone. However, the impact of the occurrence of the 21 June large earthquake and its aftershocks sequence during this one-

week forecasting interval should be considered when appraising the model performance. For detail information about the characteristics of the prior and posterior distribution of the ETAS model parameters, please see [17, 43].

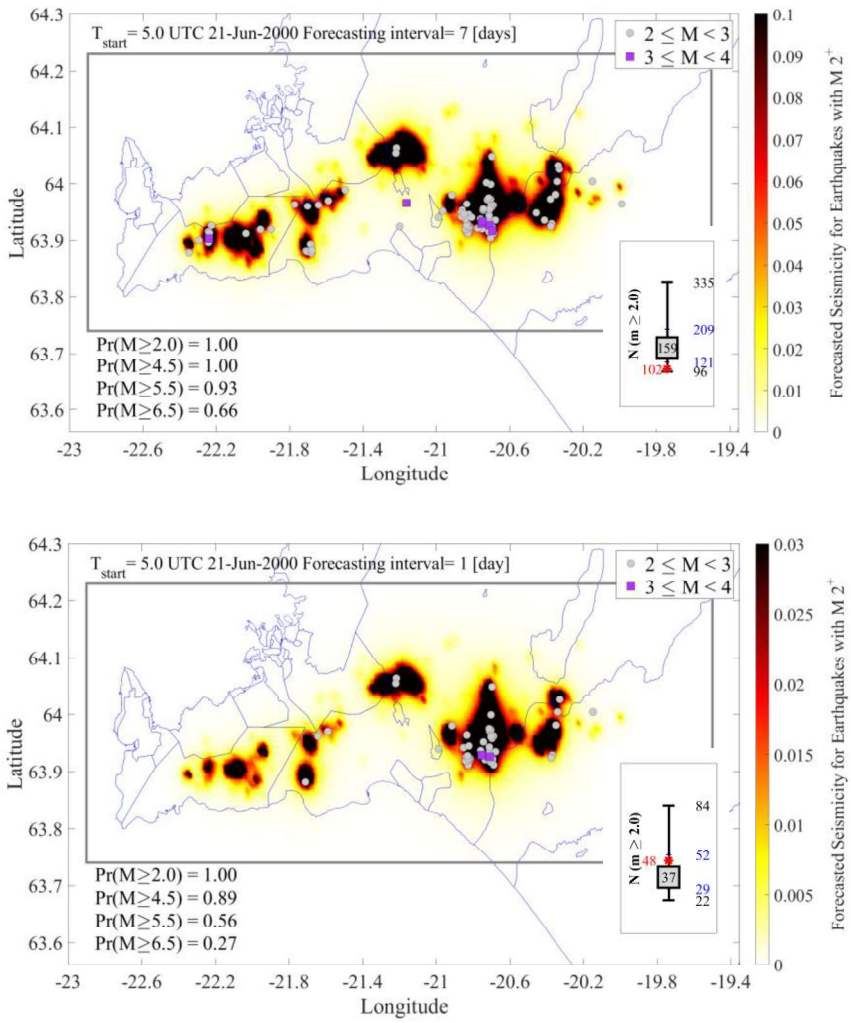

Fig. 4 – Weekly (top map) and daily (bottom map) seismicity forecasts map for events with $M_w \geq 2.0$ across SISZ and RPOR following the 21 June 2000 large earthquake. The forecasting intervals start ~4 hours after the occurrence of the mainshock. The figure description is similar to Fig. 3.

It should be emphasized that although we presented the seismicity forecasts map for events with $M_w \geq 2.0$, the estimates corresponding to $M_w \geq 4.5$ is used for the hazard calculation to be comparable with the conventional hazard values obtained from the ESHM13.

4.2 Short-term seismic hazard results

Fig. 5 and Fig. 6 show the ratio of the short-term hazard curve to the conventional (long-term) hazard curve at Hveragerði site following 17 and 21 June large earthquakes, respectively. The forecasted aftershock hazard curves for PGA thresholds calculated from individual GMPEs of RS09 (dashed lines) and Kea20 (solid lines). In both figures, the left and right-side panels correspond to the one-week and one-day forecasting time interval, respectively. The hazard values correspond to the rate of exceeding a set of prescribed PGA thresholds. The hazard curves obtained from the short-term PSHA (i.e., daily and weekly forecasted hazard values calculated by seismicity forecasts of the ETAS model) indicate a significant increase in the daily rate of exceedance compared to the ones from the conventional hazard values across

PGA thresholds. This can be observed for both daily and weekly forecasting intervals. The observation is consistent with our expectation that the aftershock hazard increases significantly immediately following a large mainshock and the Bayesian ETAS model can account for the seismicity increase in the affected area.

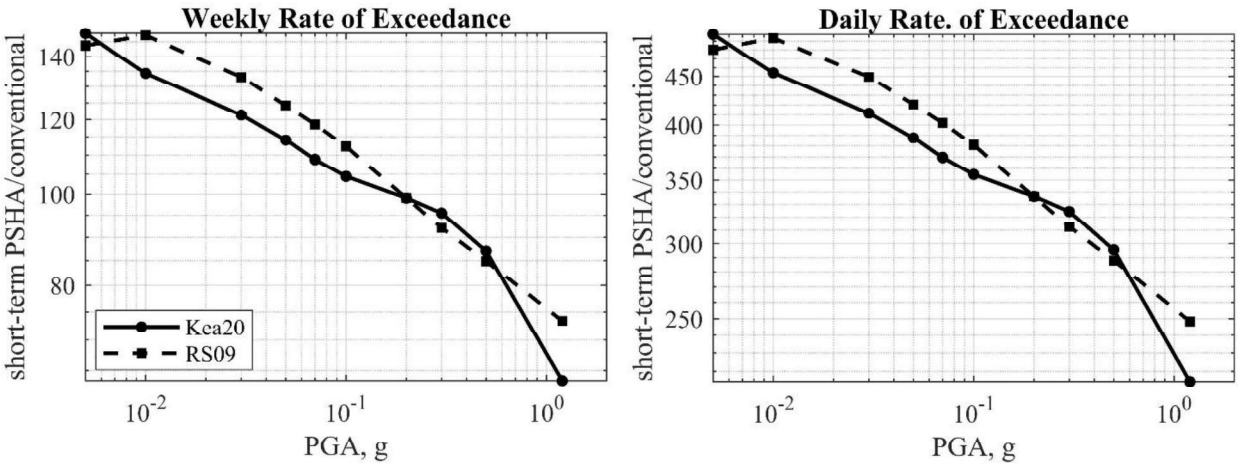

Fig. 5 – The short-term to conventional (long-term) ratio of seismic hazard values for PGA following the 17 June mainshock at Hveragerði site. The short-term hazard values are based on the seismicity forecasts obtained from the Bayesian ETAS model corresponding to one-week and one-day forecasting intervals.

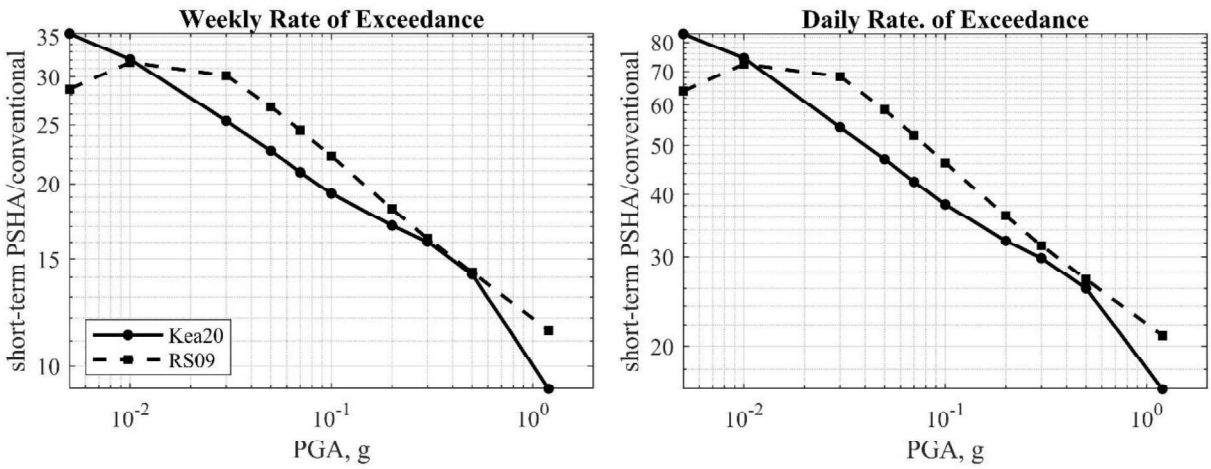

Fig. 6 –The short-term to conventional (long-term) ratio of seismic hazard values for PGA following the 21 June earthquake at Hveragerði site in the SISZ. The caption is similar to Fig. 5.

The ratio of the short-term hazard values to the conventional hazard values obtained from the long-term seismicity rate (i.e., SEIFA model), known as the probability gain, decreases gradually as PGA increases. The daily exceedance rate of 0.3g is estimated $3.5 \cdot 10^{-4}$ by the conventional hazard assessment, while in the short-term PSHA, the forecasted daily exceedance rate of 0.3g is 10^{-2}. This means that in the aftershock time interval, the daily exceedance rate of PGA increases by a factor of ~30 relative to the conventional hazard value. Also, the factor of 30 at 0.3g can be observed in the right panel of Fig. 6, corresponding to the daily forecasting interval starting 4 hours after the 21 June earthquake.

The same comparison for forecasting intervals starting after the 17 June event (see Fig. 5) indicates ten times larger probability gain values (i.e., ~factor of 300) compared to the probability gain assessed following the 21 June mainshock (Fig. 6). This is mainly due to the large number of aftershocks that followed the first mainshock, as well as the larger number of moderate-to-large magnitude events (see right panel of Fig. 1).

As visible from both figures, compared to Kea20, RS09 shows a larger probability of gain across almost all PGA thresholds for daily and weekly forecasting intervals. PGA estimates with various exceedance rate obtained from the RS09 are larger than those by the Kea20. This was observed in both short-term and conventional hazard assessment. Note that an important characteristic of RS09 is that it predicts a relatively high PGA in the near-fault area (short distances of cells surrounding the hazard site) while the decay with distance is faster than resultant from the regional GMPEs. Also, the high PGAs can be explained by shallow earthquakes (< 10 km) in the SISZ. Note that the fast decay with distance in Iceland was addressed by the existence of young, fractured and relatively weak rock in the SISZ that dampens the propagating seismic waves faster than in more solid rock.

5. Summary and Conclusion

To evaluate the feasibility of OEF for aftershocks in SW-Iceland following large-magnitude earthquakes and using the location of the town Hveragerði for determining the evolving seismic hazard by conducting short-term seismic hazard assessment, we carried out a retrospective forecasting experiment using a major seismic sequence that occurred in the SISZ in June 2000. For this purpose, we compute the space-time seismicity forecasts across the SISZ and RPOR (defined as the aftershock zone) for one-day and one-week forecasting intervals starting ~4 hours after the occurrence of the 17 June (M_w6.4) and 21 June (M_w6.5) mainshocks. To this end, an advanced Bayesian spatio-temporal ETAS model, which showed promising results in modelling the 2016 Amatrice seismic sequence in central Italy [2], was employed. The model exploits the Bayesian inference framework and Markov Chain Monte Carlo simulations for adaptively learning the ETAS parameters based on data from the ongoing seismic sequence. The spatial distribution of the 50th percentile of the forecasts was illustrated for the forecasting intervals of interest and compared with the observed earthquakes taking place during the desired forecasting interval across the aftershock zone. Moreover, using Bayesian parameter estimation allowed us to report the estimated number of events with magnitude larger than or equal to the lower cut-off magnitude through an error-bar illustration, presenting the median, 16th, 84th, 2nd and 98th percentiles of forecasts across the SW-Iceland. The results indicate that the ETAS model is capable of forecasting the increase in seismicity after a strong earthquake as well as its spatial distribution, and short (i.e., daily time intervals) forecasting intervals are preferable for the potential OEF system in SW-Iceland.

Finally, we obtained the short-term hazard values (i.e., the rate of exceeding PGA thresholds) at Hveragerði using local GMPEs. To evaluate the level of increase in the seismic hazard values during an intense seismic activity in SW-Iceland, we presented the ratio of the short-term rate of exceeding PGA values to their corresponding long-term seismic hazard values (i.e., conventional PSHA based on the ESHM13 model). The comparison shows that for the one-week forecasting interval following the 17 June earthquake and 21 June earthquake, the short-term hazard values increase by a factor of 60-150 and 10-35, respectively. Moreover, in SW-Iceland, the shorter forecasting time interval results in a higher probability gain.

6. Acknowledgements

This study was funded by the Horizon 2020 TURNkey project [https://earthquake-turnkey.eu/] (Towards more Earthquake-Resilient Urban Societies through a Multi-Sensor-Based Information System enabling Earthquake Forecasting, Early Warning and Rapid Response Actions), under grant agreement No 821046. This work was also funded by a Postdoctoral fellowship (No. 218255-051) from the Icelandic Research Fund of the Icelandic Centre for Research.

7. References

[1] Ogata Y. (1988): Statistical models for earthquake occurrences and residual analysis for point processes. *Journal of the American Statistical Association*, 83(401), 9–27.

[2] Ebrahimian H, Jalayer F. (2017): Robust seismicity forecasting based on Bayesian parameter estimation for epidemiological spatio-temporal aftershock clustering models. *Sci Rep*, 7(1), 9803.
[3] McGuire RK. (2004) Seismic hazard and risk analysis. Earthquake engineering research institute.
[4] Woessner J, Laurentiu D, Giardini D, Crowley H, Cotton F, Grünthal G, et al. (2015): The 2013 European seismic hazard model: key components and results. *Bulletin of Earthquake Engineering*, 13(12), 3553–3596.
[5] Kowsari M, Sonnemann T, Halldorsson B, Hrafnkelsson B, Snæbjörnsson JÞ, Jónsson S. (2020): Bayesian Inference of Empirical Ground Motion Models to Pseudo-Spectral Accelerations of South Iceland Seismic Zone Earthquakes based on Informative Priors. *Soil Dynamics and Earthquake Engineering*, 132, 106075.
[6] Rupakhety R, Sigbjörnsson R. (2009): Ground-motion prediction equations (GMPEs) for inelastic response and structural behaviour factors. *Bull Earthquake Eng*, 7(3), 637–659.
[7] Jordan TH, Chen YT, Gasparini P, Madariaga R, Main I, Marzocchi W, et al. (2011): Operational earthquake forecasting: State of knowledge and guidelines for utilization. *Annals of Geophysics*, 54(4), 319–391.
[8] Marzocchi W, Lombardi AM, Casarotti E. (2014): The Establishment of an Operational Earthquake Forecasting System in Italy. *Seismological Research Letters*, 85(5), 961–969.
[9] Nandan S, Ouillon G, Wiemer S, Sornette D. (2017): Objective estimation of spatially variable parameters of epidemic type aftershock sequence model: Application to California: Spatially Variable Parameters of ETAS. *J. Geophys. Res. Solid Earth*, 122(7), 5118–5143.
[10] Taroni M, Marzocchi W, Schorlemmer D, Werner MJ, Wiemer S, Zechar JD, et al. (2018): Prospective CSEP Evaluation of 1-Day, 3-Month, and 5-Yr Earthquake Forecasts for Italy. *Seismological Research Letters*, 89(4), 1251–1261.
[11] Gerstenberger M, McVerry G, Rhoades D, Stirling M. (2014): Seismic Hazard Modeling for the Recovery of Christchurch. *Earthquake Spectra*, 30(1), 17–29.
[12] Field EH, Biasi GP, Bird P, Dawson TE, Felzer KR, Jackson DD, et al. (2015): Long-term time-dependent probabilities for the third uniform California earthquake rupture forecast (UCERF3). *Bulletin of the Seismological Society of America*, 105(2), 511–543.
[13] Ebrahimian H, Jalayer F, Asprone D, Lombardi AM, Marzocchi W, Prota A, et al. (2014) Adaptive Daily Forecasting of Seismic Aftershock Hazard. *Bulletin of the Seismological Society of America*, 104(1), 145–161.
[14] Lombardi AM. (2015) Estimation of the parameters of ETAS models by simulated annealing. *Scientific Reports*, 5, 8417.
[15] Lombardi AM. (2017): The epistemic and aleatory uncertainties of the ETAS-type models: an application to the Central Italy seismicity. *Scientific reports*, 7(1), 11812.
[16] Cornell CA. (1968): Engineering seismic risk analysis. *Bulletin of the Seismological Society of America*, 58(5), 1583–1606.
[17] Darzi A, Hrafnkelsson B, Halldorsson B, Ebrahimian H, Jalayer F. (2021): Calibration of a Bayesian Spatio-temporal ETAS Model to the June 2000 South Iceland Seismic Sequence. *In Review*.
[18] Hardebeck JL, Llenos AL, Michael AJ, Page MT, van der Elst N. (2019): Updated California Aftershock Parameters. *Seismological Research Letters*, 90(1), 262–270.
[19] Reasenberg, Jones. (1989): Earthquake Hazard After a Mainshock in California. *Science*, 243(4895), 1173–1176.
[20] Llenos AL, Michael AJ. (2019): Ensembles of ETAS Models Provide Optimal Operational Earthquake Forecasting During Swarms: Insights from the 2015 San Ramon, California Swarm. *Bulletin of the Seismological Society of America*, 109(6), 2145–2158.
[21] Shcherbakov R, Zhuang J, Zöller G, Ogata Y. (2019): Forecasting the magnitude of the largest expected earthquake. *Nat Commun*, 10(1), 4051.
[22] Kowsari M, Halldorsson B, Hrafnkelsson B, Jonsson S. (2019): Selection of earthquake ground motion models using the deviance information criterion. *Soil Dynamics and Earthquake Engineering*, 117, 288–299.
[23] Kowsari M, Halldorsson B, Snæbjörnsson JÞ, Jónsson S. (2021): Effects of Different Empirical Ground Motion Models on Seismic Hazard Maps for North Iceland. *Soil Dynamics and Earthquake Engineering*.
[24] Sigbjörnsson R, Snæbjörnsson JTh, Higgins SM, Halldorsson B, Ólafsson S. (2009): A note on the Mw 6.3 earthquake in Iceland on 29 May 2008 at 15:45 UTC. *Bull Earthquake Eng*, 7(1), 113–126.
[25] Halldorsson B, Sigbjörnsson R. (2009): The Mw6. 3 Ölfus earthquake at 15: 45 UTC on 29 May 2008 in South Iceland: ICEARRAY strong-motion recordings. *Soil Dynamics and Earthquake Engineering*, 29(6), 1073–1083.
[26] Panzera F, Zechar JD, Vogfjörd KS, Eberhard DAJ. (2016): A Revised Earthquake Catalogue for South Iceland. *Pure Appl. Geophys.*, 173(1), 97–116.
[27] Einarsson P, Hjartardóttir ÁR, Hreinsdóttir S, Imsland P. (2020): The structure of seismogenic strike-slip faults in the eastern part of the Reykjanes Peninsula Oblique Rift, SW Iceland. *Journal of Volcanology and Geothermal Research*, 391, 106372. Elsevier.

[28] Steigerwald L, Einarsson P, Hjartardóttir ÁR. (2020): Fault kinematics at the Hengill Triple Junction, SW-Iceland, derived from surface fracture pattern. *Journal of Volcanology and Geothermal Research*, 391, 106439.
[29] Einarsson P. (2014): Mechanisms of Earthquakes in Iceland. In Beer M, Kougioumtzoglou IA, Patelli E, Au IS-K (eds). *Encyclopedia of Earthquake Engineering*, Berlin, Heidelberg: Springer Berlin Heidelberg. pp.1–15.
[30] Beck JL, Au S-K. (2002): Bayesian updating of structural models and reliability using Markov chain Monte Carlo simulation. *Journal of engineering mechanics*, 128(4), 380–391. American Society of Civil Engineers.
[31] Jalayer F, Ebrahimian H. (2014): MCMC-based Updating of an Epidemiological Temporal Aftershock Forecasting Model. In *Vulnerability, Uncertainty, and Risk*, Liverpool, UK: American Society of Civil Engineers. pp.2093–2103.
[32] Metropolis N, Rosenbluth AW, Rosenbluth MN, Teller AH, Teller E. (1953): Equation of state calculations by fast computing machines. *The journal of chemical physics*, 21(6), 1087–1092.
[33] Hastings WK. (1970): Monte Carlo sampling methods using Markov chains and their applications. *Biometrika*, 57(1), 97–109.
[34] Cotton F, Scherbaum F, Bommer JJ, Bungum H. (2006): Criteria for selecting and adjusting ground-motion models for specific target regions: Application to central Europe and rock sites. *Journal of Seismology*, 10(2), 137–156.
[35] Bommer JJ, Douglas J, Scherbaum F, Cotton F, Bungum H, Fäh D. (2010): On the selection of ground-motion prediction equations for seismic hazard analysis. *Seismological Research Letters*, 81(5), 783–793.
[36] Woessner J, Laurentiu D, Giardini D, Crowley H, Cotton F, Grünthal G, et al. (2015): The 2013 European Seismic Hazard Model: key components and results. *Bulletin of Earthquake Engineering*, 13(12), 3553–3596. Springer Netherlands.
[37] Árnadóttir T. (2004): Coseismic stress changes and crustal deformation on the Reykjanes Peninsula due to triggered earthquakes on 17 June 2000. *Journal of Geophysical Research*, 109(B9).
[38] Stefansson R, Bonafede M, Gudmundsson GB. (2011): Earthquake-Prediction Research and the Earthquakes of 2000 in the South Iceland Seismic Zone. *Bulletin of the Seismological Society of America*, 101(4), 1590–1617.
[39] Einarsson P. (1991): Earthquakes and present-day tectonism in Iceland. *Tectonophysics*, 189(1), 261–279.
[40] Einarsson P. (2010): Mapping of Holocene surface ruptures in the South Iceland Seismic Zone. *Jökull*, 60, 121–138.
[41] Einarsson P. (2014): Mechanisms of Earthquakes in Iceland. In Beer M, Kougioumtzoglou IA, Patelli E, Au IS-K (eds). *Encyclopedia of Earthquake Engineering*, Berlin, Heidelberg: Springer Berlin Heidelberg. pp.1–15.
[42] Sigmundsson F. (2006): Iceland geodynamics: crustal deformation and divergent plate tectonics. Springer Science & Business Media.
[43] Darzi A, Ebrahimian H, Halldorsson B, Jalayer F. (2021): Retrospective seismicity forecasting of the 17 and 21 June 2000 South Iceland earthquakes by a Bayesian epidemiological type spatio-temporal aftershock clustering model. In *The 13th International Conference on Structural Safety and Reliability (ICOSSAR 2021),* Shanghai, P.R. China: ICOSSAR. p.1.

